Journal of the Physical Society of Japan
Vol. 59, No. 4, April, 1990, pp. 1232–1241

RFP Plasma Performance in the *F-Θ* Pumping Experiments on ZT-40M

Shunjiro SHINOHARA,* Kurt F. SCHOENBERG, John C. INGRAHAM, Carter P. MUNSON, Paul G. WEBER, Don A. BAKER, Robert F. GRIBBLE, William A. REASS, Aldred E. SCHOFIELD and Glen A. WURDEN

Los Alamos National Laboratory, Los Alamos, New Mexico 87545, U.S.A.

(Received July 5, 1989)

Plasma performance in the *F-Θ* pumping condition has been studied on the reversed field pinch (RFP) device ZT-40M. Compared with an un-modulated case, slight changes of plasma parameters are found for the case of current drive phasing. On the other hand, the increases in radiated power and impurity intensity, and the decreases in plasma current and soft X ray intensity are observed for the anti-drive phasing. Changes of effective minor radius, inferred internal structures and phases between various plasma parameters during modulation are also studied. Frequency spectra up to the 10th harmonic of the driving frequency (1.3 and 2 kHz) are investigated. The fast penetration (>10 kHz) of changes of plasma parameters to the central region and the increased impurity and soft X ray intensities with an increase in the frequency are found.

§1. Introduction

In toroidal devices such as the tokamak and reversed field pinch (RFP), plasma confinement is maintained, in part, by a poloidal magnetic field generated by the toroidal current in the plasma. For steady-state operation, a method of continuously driving the toroidal current is necessary, and a variety of methods have been proposed.[1-5]

In an RFP device, toroidal and poloidal winding currents are nonlinearly coupled by the plasma, so there is a possibility of sustaining the mean plasma current with proper time dependent programming of the toroidal and poloidal loop voltages.[6-8] This technique of oscillating field current drive (OFCD), also known as *F-Θ* pumping, could be very useful for a reactor plasma. (Here, F and Θ are the ratio of the toroidal field at the wall $B_{\phi w}$ to the mean toroidal field $\langle B_\phi \rangle$, and the ratio of the poloidal field at the wall $B_{\theta w}$ to $\langle B_\phi \rangle$, respectively.)

The experiment of modulating the toroidal or poloidal field circuit individually has been performed in the ZT-40M device at Los Alamos National Laboratory.[9] Results for modulation of a single field component were compared with the theoretical predictions, and did not indicate any adverse effect on the plasma, provided toroidal field reversal was adequately maintained. Initial experimental results of *F-Θ* pumping (simultaneous modulating both the toroidal and poloidal field coil currents with a phase control between the currents (dual drive)) are studied[10,11] in order to demonstrate and assess the potentials of the current drive. In this paper, we focus on RFP plasma performance including a power spectral analysis, i.e., plasma response and physical pictures, in the *F-Θ* pumping condition on the ZT-40M. In §2, time behavior of RFP discharges is summarized for near optimum phasing between the toroidal and poloidal field circuits (current drive direction), for anti-current drive phasing (180° from optimum) and for the undriven conditions. We have measured the plasma response to the field modulation, and examine the effects of this on RFP performance. Due to the nonlinear coupl-

* On leave of absence from Department of Physics, Faculty of Science, University of Tokyo, Bunkyo-ku, Tokyo 113.

ing of the currents of the toroidal and poloidal field coils, there exist higher harmonic components of the driving frequency. In §3, we provide results of an analysis of these components of the plasma parameters driven by the circuit and the plasma. Finally, conclusions are described in §4.

§2. RFP Discharges with *F-Θ* Pumping

In this section, we discuss the temporal behavior of $I_\phi = 160$ kA (plasma current) modulated discharges that are subsequently analyzed in §3. A complete discussion of the overall ZT-40M *F-Θ* pumping experiments appears in ref. 11.

Typical machine and plasma parameters for the *F-Θ* pumping discharges discussed in this paper are as follows; major radius $R = 114$ cm, minor radius $a = 20$ cm, plasma current $I_\phi \sim 160$ kA, line-averaged plasma density $\bar{n}_e \sim 2 \times 10^{13}$ cm^{-3}, central electron temperature $T_e(0) \sim 330$ eV, ion temperature $T_i \sim 250$ eV. Applied modulation voltages (peak to peak values) of the toroidal and poloidal directions are less than ~ 800 V and ~ 40 V, respectively, with modulation applied for ~ 12 ms. As for the *F-Θ* pumping circuits, a block diagram for the dual drive of the toroidal and poloidal field coils with a phase control is shown in Fig. 1. The poloidal (toroidal) field oscillator is connected in series with the poloidal (toroidal) capacitor bank with the use of ML8618 power triode tubes (operated class D).

Figure 2 shows a typical example of the time evolution of the plasma current I_ϕ and total radiated power P_r measured by the bolometer,[12] for conditions of near optimum phasing (current drive direction; shot number 21237), phase difference of 180° from optimum phasing (anti-current drive direction; shot number 21238) and the undriven reference (shot number 21244) conditions. Here, the driving frequency is 2 kHz and we will mainly use these three typical shots afterwards unless denoted. For the current drive phasing, both I_ϕ and P_r change very little in comparison to the case without the modulation. On the other hand, for the anti-drive phasing, a decrease in I_ϕ and an increase in P_r are observed. For this phasing, the impurity intensity of CrI near the wall also increases. The plasma resistivity, η_k, defined from the helicity balance[13] is also larger for the anti-drive case. In all cases, the centering of the plasma column changes little both radially and vertically ($\lesssim 0.1$ cm).

Figure 3 shows the time evolution of the plasma current I_ϕ, toroidal loop voltage V_ϕ, poloidal loop voltage V_θ, line-averaged plasma density $\bar{n}_e$, toroidal field at the wall $B_{\phi w}$, mean toroidal field $\langle B_\phi \rangle$ and the input drive power (Poynting vector) P from $t = 5$ to 10 ms, for the same shots as in Fig. 2. Note that the modulation is superimposed on the ohmic (unmodulated) condition in both V_θ and V_ϕ signals. The modulation amplitudes of I_ϕ, V_ϕ

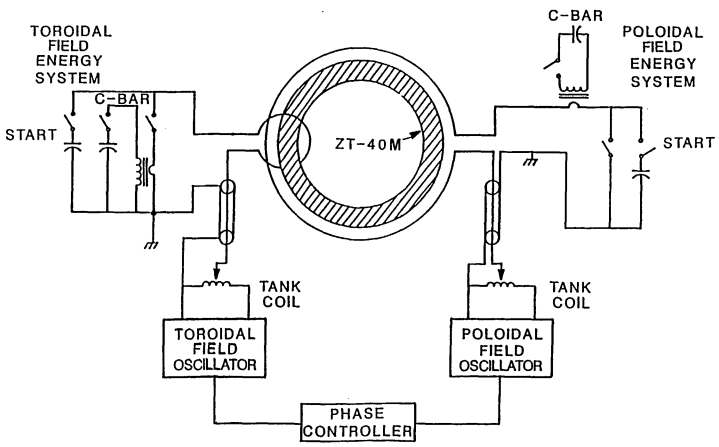

Fig. 1. Block diagram of modulating both the toroidal and poloidal field coil currents with a phase control.

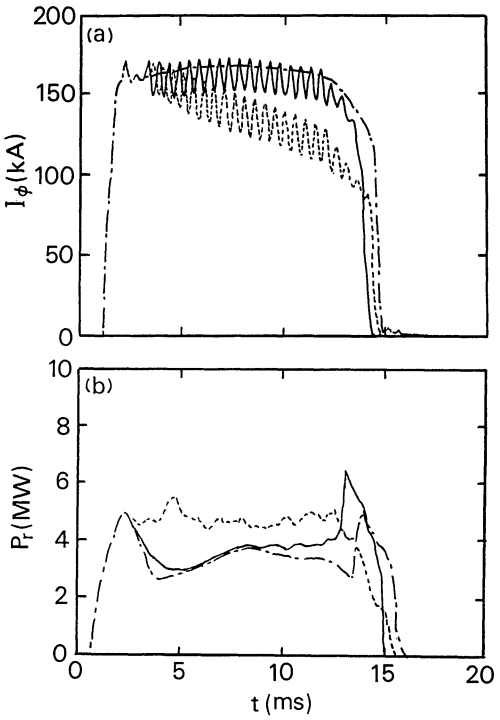

Fig. 2. Time evolution of (a) plasma current I_ϕ and (b) total radiated power P_r for drive (solid lines), anti-drive (dotted lines) and unmodulated (dotted-dashed lines) cases.

and $\langle B_\phi \rangle$ are smaller, but that of $B_{\phi w}$ is larger with the drive phase in comparison to those with the anti-drive phase (see also Fig. 4). The V_θ signals are somewhat noisier than the other signals; high frequency components (>20 kHz with a typical amplitude of ±0.3 V) are filtered out in this figure. The peak to peak modulation power for both drive and anti-drive cases is ~110 MW. The average values of this input power are about 7.5 MW for drive and unmodulated cases and 8.0 MW for anti-drive case.

The total flux consumption for the iron core during shots for the drive case is a little larger than that without the modulation, and this consumption is smaller than that for the anti-drive case by ~30%, which comes from the larger plasma resistance for this anti-drive case. The resistance and plasma wall interaction become larger compared with the low current (I_ϕ=60–70 kA) and low power modulation (P~18 MW peak to peak) case.[11] As is the same with the results in ref. 11, this in-

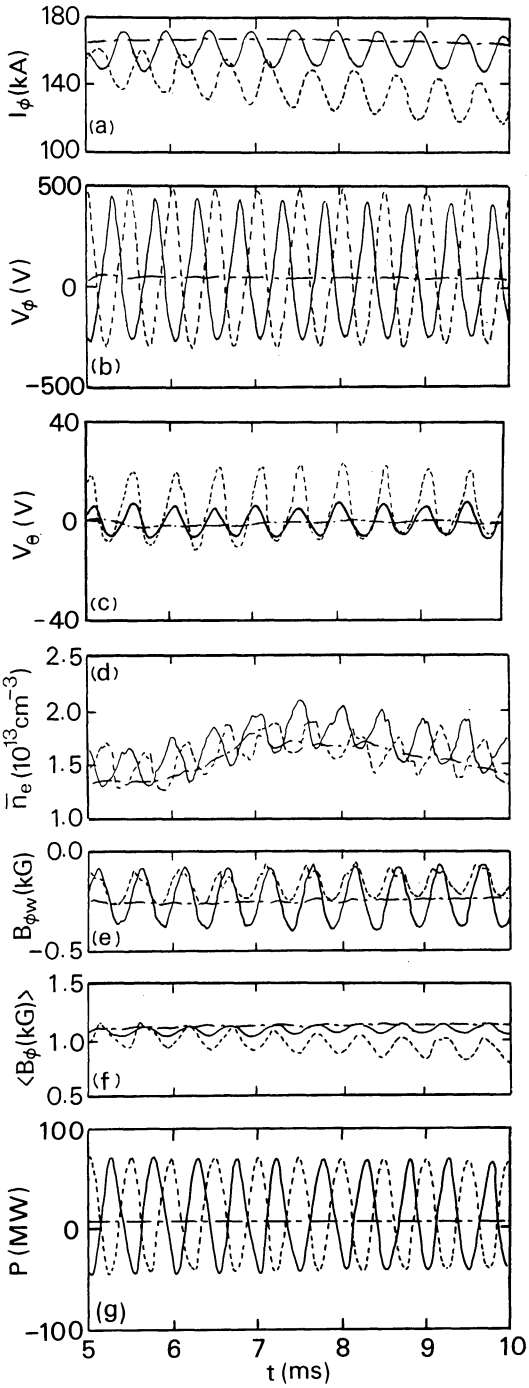

Fig. 3. Time evolution of (a) plasma current I_ϕ, (b) toroidal loop voltage V_ϕ, (c) poloidal loop voltage V_θ (high frequency components are filtered out), (d) line-averaged plasma density $\bar{n}_e$, (e) toroidal field at the wall $B_{\phi w}$, (f) mean toroidal field $\langle B_\phi \rangle$ and (g) input drive power (Poynting vector) P from t=5 to 10 ms. The line types are the same with those in Fig. 2.

crease in the plasma resistance with $I_\phi \sim 160$ kA reduces the observable current drive effects for the current drive case. In addition, the main reason of the decrease in the plasma current for the anti-drive case is this increased resistance rather than that expected from the helicity extraction: If the plasma resistivity η scales as $I_\phi^{-0.85}$ as described in ref. 14, the loop voltage V_ϕ becomes nearly constant, which cannot explain the enhanced flux consumption. (Even though η scales as $I_\phi^{-1.5}$, V_ϕ is expected to increase by less than 10%). The increases in the radiation loss as shown in Fig. 2(b) and CrI intensity and also the decrease in the soft X ray emissivity (mainly due to a decrease in the electron temperature; see Fig. 5) correlate with this (observed) increased resistance.

F-Θ trajectories for the drive, anti-drive and unmodulated cases are shown in Fig. 4. For the current drive case, the *F-Θ* trajectory is nearly along a straight line with a narrow width. However, the trajectory for the anti-drive case shows different behaviors to have a large excursion to increase the Θ value in the deep reversal phase with F is nearly constant and to deviate from a Bessel function model (BFM), i.e., the substantial decrease in the minor radius (see Fig. 6). These different behaviours may indicate the different plasma dynamics in the *F-Θ* diagram between the two cases. For the previous single drive experiment[9] (modulation of V_ϕ or V_θ), this width is narrower than the anti-drive case, and somewhat wider than the drive case. However, both single and dual modulation (drive direction) experiments have shown that the plasma remained nearly relaxed on a unique *F-Θ* trajectory with the toroidal field reversed.

Figure 5 shows radial distributions of soft X ray emissivity above 600 eV detected by surface barrier diodes[15] with the use of filters at $t=8$ ms. Mean intensity for the drive case decreases a little compared with the unmodulated case, but this intensity for the anti-drive case decreases by up to $\sim 80\%$ of that without the modulation mainly due to a decrease in the electron temperature.

Next, the possibility of a change of minor radius during the modulation is considered. We estimate the minor radius in two ways. (In both ways, the minor radius is defined so as to match the parameters measured outside the plasma, using the pressure balance equation with some assumptions.) One is to calculate a break point radius α from a modified Bessel function model (MBFM);[16] a modified force-free equation of $\nabla \times B = \lambda(r)B$ is used, where B is a magnetic field and λ is constant from $r=0$ to αa and decreases linearly with radius from $r=\alpha a$ to a (λ is zero at a). Another is the use of the pressure balance with surface current model; surface toroidal and poloidal plasma currents at $r=a_{\mathrm{eff}}$ are assumed. (The poloidal field inside the plasma is zero, and this field outside plasma surface is finite and decreases with the minor radius of r. The toroidal field B_ϕ is defined as $B_{\phi\mathrm{eff}}$ for $0 \le r < a_{\mathrm{eff}}$ and as $B_{\phi w}$ at $a_{\mathrm{eff}} < r \le a$.) Both a_{eff} and $B_{\phi\mathrm{eff}}$ are derived from the magnetic pressure balance equation at $r=a_{\mathrm{eff}}$ and from measured toroidal flux Φ, B_ϕ and I_ϕ. Note that there is a clear correlation be-

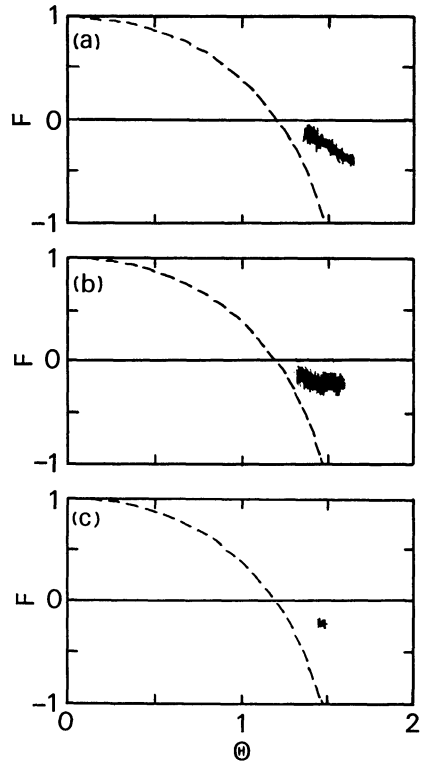

Fig. 4. *F-Θ* trajectories for (a) drive ($t=7$–11 ms), (b) anti-drive ($t=5$–8 ms) and (c) unmodulated ($t=8$–12 ms) cases. Dashed lines show a Bessel function model.

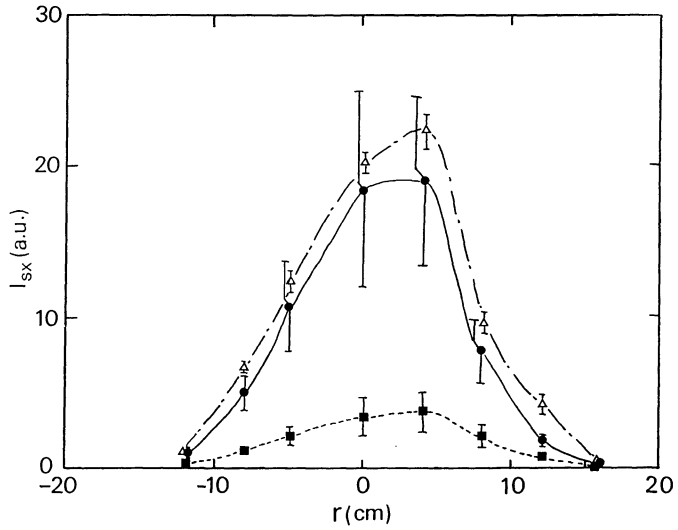

Fig. 5. Radial profiles of soft X ray emissivity for drive (solid line with closed circles), anti-drive (dotted line with closed boxes) and unmodulated (dashed and dotted line with open triangles) cases at $t=8$ ms. Error bars are described to show the maximum and minimum values of soft X ray emissivity from $t=7.5$ to 8.5 ms.

tween a_{eff} and α (see Fig. 6) due to the same input values, i.e., Φ, B_ϕ and I_ϕ, to derive these two parameters. Summing up, both α and a_{eff} denote the "effective" minor radius (from two different definitions), in which most of the plasma current flows ($r<\alpha a$) and in which toroidal field is positive (a_{eff} is a reversal point), respectively. Therefore, reductions of α and a_{eff} mean the deviation from BFM (fully relaxed state with pressure is zero); if F is constant, Θ becomes larger compared with this BFM.

The trajectories in (a_{eff}, α) space are shown in Fig. 6 for the drive, anti-drive and unmodulated cases. During the modulation, amplitudes of a_{eff} oscillates by $\sim\pm5\%$ and $\sim\pm7\%$ for the drive ($t=7$–11 ms) and anti-drive ($t=5$–8 ms) cases, respectively. Changes of α are larger than those of a_{eff}, i.e., $\sim\pm12\%$ and $\sim\pm18\%$ for the drive and anti-drive cases, respectively. On the other hand, there are small changes of a_{eff} ($\sim\pm0.7\%$) and α ($\sim\pm1.4\%$) from $t=8$ to 12 ms for undriven condition.

We will use the parameter a_{eff} as a measure of the effective plasma radius hereafter, because we can use either a_{eff} or α as described above. The dependence of a_{eff} on Θ is shown in Fig. 7. With the increase in Θ during the modulation, the decrease in a_{eff} is observed for both drive and anti-drive cases. For the unmodulated case, a_{eff} and Θ lie between 14.6 and 14.8 cm, and 1.43 and 1.49, respectively ($t=8$–12 ms). Contrary to Fig. 7, the dependence of $B_{\phi\mathrm{eff}}$ on Θ shows different behaviors, as is shown in Fig. 8. Although nearly linear dependence is found for the drive case, the trace for the anti-drive case shows an

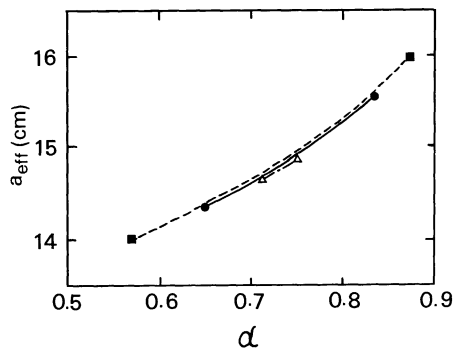

Fig. 6. Excursions in (a_{eff}, α) plane for drive ($t=7$–11 ms; solid line), anti-drive ($t=5$–8 ms; dotted line) and unmodulated ($t=8$–12 ms; dotted-dashed line) cases. Here, a_{eff} is a minor radius derived from pressure balance calculation and α is a break point radius from modified Bessel function model (MBFM).

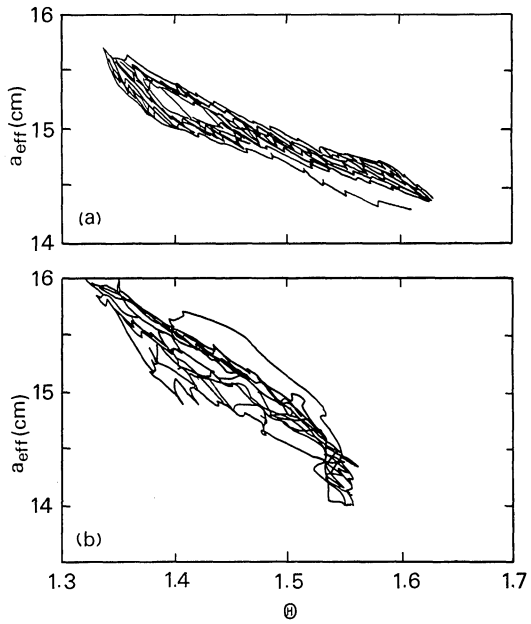

Fig. 7. Relation between effective minor radius a_{eff} from pressure balance calculation and Θ for (a) drive (t=7–11 ms) and (b) anti-drive (t=5–8 ms) cases. For drive case, traces at the low Θ side are clockwise.

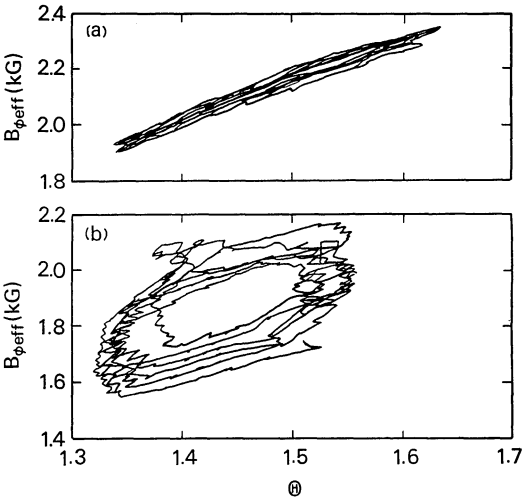

Fig. 8. Relation between effective toroidal field $B_{\phi eff}$ from pressure balance calculation and Θ for (a) drive (t=7–11 ms) and (b) anti-drive (t=5–8 ms) cases. For anti-drive case, traces are counter clockwise.

ellipse with counter clockwise rotation, which may be due to the different pushing direction in the F-Θ diagram.

In order to estimate the internal plasma properties such as the magnetic field and current density, we have used the MBFM, i.e., the use of α, under an assumption of the plasma to evolve through a series of quasi-relaxed state. In Fig. 9, radial profiles of the magnetic fields, current densities and safety factors are shown for compressed and decompressed phases for the current drive phasing. In addition, unmodulated case is also shown for comparison. As is the same phenomenon with the low current discharges (I_ϕ=60–70 kA) and fixed α value of 0.6 described in ref. 11, the magnetic field B_ϕ at the center is in phase opposition to that at the plasma edge and also to F value. The toroidal j_ϕ and poloidal j_θ current densities near the center are in phase opposition to those near the edge, too. The plasma current I_ϕ is in phase with B_ϕ at the center and Θ, but I_ϕ is in phase opposition to α, F, CrI and D_α intensities. Therefore, the current densities of j_ϕ and j_θ contract with a reduction of safety factor q at the center and with a decrease in impurity intensity due to the reduction of plasma wall interaction (because of the smaller minor radius).

For the case with the increased amplitude of the modulated poloidal voltage V_θ, the plasma current decreases and toroidal flux increases when the toroidal field at the wall $B_{\phi w}$ becomes nearly zero. When we increase the field reversal and increase the amplitude of V_θ, good plasma discharges are not obtained due to the presence of giant sawteeth for the condition of $\Theta > 1.6$ (see §3).

For a driving frequency of 1.3 kHz, we also have the same plasma behavior for that of the 2 kHz modulation described above. For the purpose of understanding plasma behavior in the present experiments, simulations developed from ref. 15 have been done for the same experimental conditions. Results of the simulations are in good agreement with the experiments (especially for low power modulation case), which helps to demonstrate the F-Θ pumping technique.

§3. Analysis of Higher Harmonics

In the previous section, we have analyzed plasma parameters with a driving frequency of typically 2 kHz. In the currents of the toroidal and poloidal field coils, there exist higher har-

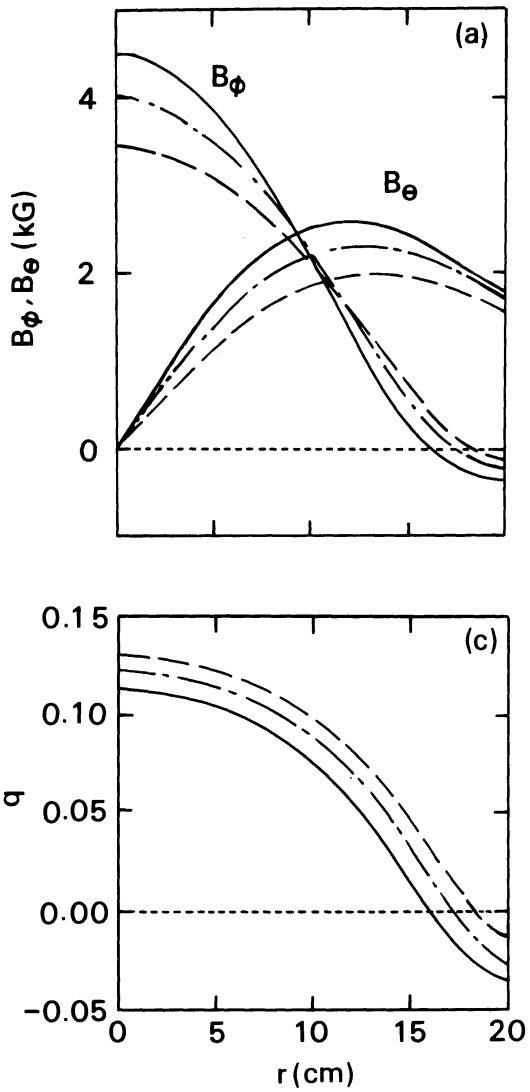

Fig. 9. Radial profiles of (a) toroidal field B_ϕ and poloidal field B_θ, (b) toroidal j_ϕ and poloidal j_θ current densities and (c) safety factor q for the drive case. Solid and broken lines denote compressed ($\Theta=1.62$, $F=-0.35$ and $\alpha=0.67$ at t 7.9 ms) and decompressed ($\Theta=1.36$, $F=-0.08$ and $\alpha=0.83$ at $t=8.15$ ms) phases. respectively. Dotted-dashed lines show unmodulated case ($\Theta=1.47$, $F=-0.21$ and $\alpha=0.77$ at $t=8.0$ ms), for comparison.

monic components of the driving frequency, although no harmonic components are found in the absence of the plasma. Using the fast Fourier transform (FFT) method with a Hamming window, power spectra of some plasma parameters are derived; the sampling number is typically 1024 with a sampling duration of 3–5 ms. In some cases, up to the 10th harmonics of the driving frequency is found in the plasma current, toroidal loop voltage and soft X ray emissivity.

Figure 10 shows the Fourier power spectra of the plasma current I_ϕ, loop voltage V_ϕ and soft X ray emissivity $I_{sx}(0)$ of the central chord ($r=0$ cm) for the drive and unmodulated cases. For the drive case, up to the 10th harmonics ($f=20$ kHz) of I_ϕ and V_ϕ and up to the 5th harmonics of $I_{sx}(0)$ are found. The valley levels of power spectra, i.e., at $(2n-1)$ kHz (n: integer), are about $-(20\text{–}60)$ dB for V_ϕ and I_ϕ, and about $-(20\text{–}40)$ dB for $I_{sx}(0)$. Without a modulation, there are no clear peaks of plasma parameters except for DC component. As for parameters such as $B_{\phi w}$, $\langle B_\phi \rangle$ and V_θ, there are no well defined peaks at the frequency greater than 6 kHz.

Figure 11 shows a radial profile of the soft X ray emissivity for the drive case. Here, this

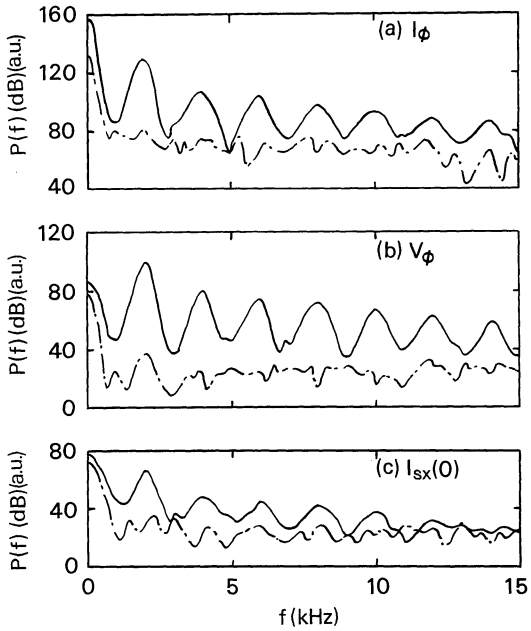

Fig. 10. Fourier power spectra of (a) plasma current I_ϕ, (b) toroidal loop voltage V_ϕ and (c) soft X ray emissivity at the plasma center $I_{sx}(0)$ for drive case (solid lines) and unmodulated case (dotted-dashed lines).

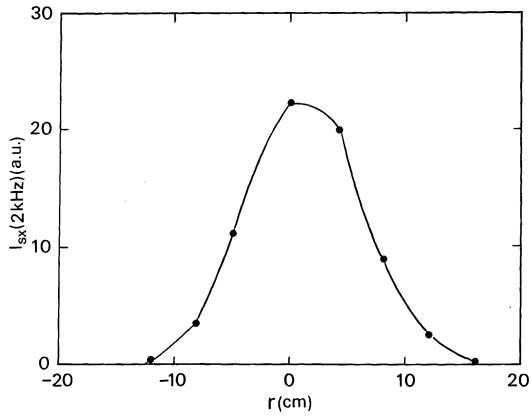

Fig. 11. Radial profile of Fourier component of soft X ray emissivity at 2 kHz fundamental oscillation for drive case.

signal represents the Fourier component at 2 kHz fun-damental oscillation. This profile is similar to the DC components of the drive and unmodulated cases in Fig. 5.

Figure 12 shows the peak plots of the Fourier power spectra normalized by the toroidal loop voltage V_ϕ at a harmonic frequency of $f=2n$ kHz for the drive case; the plasma current I_ϕ/V_ϕ, which is connected with the current driving efficiency, soft X ray emissivity I_{sx}/V_ϕ measured from minor radius $r=-12$ to 12 cm and CrI impurity intensity I_{CrI}/V_ϕ near the wall on two toroidal locations. Here, each signal of 0 dB is taken at the fundamental frequency of 2 kHz. Although the amplitude of V_ϕ decreases with the frequency f, I_ϕ/V_ϕ does not seem to depend on f. On the other hand, I_{sx} increases with the increase in f near the plasma boundary, and the increasing rate decreases when the emission comes from near the plasma center. The soft X ray emissivities (higher harmonics) of different chords are nearly in phase with each other. The normalized impurity intensities such as CrI near the plasma boundary also increase rapidly with the frequency, but non-axisymmetry distribution has been observed (see Fig. 12(c)).

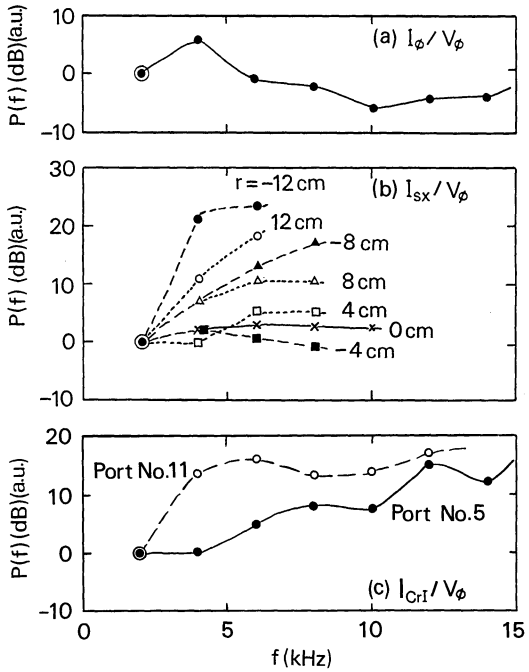

Fig. 12. Peak plots of normalized Fourier power spectra (harmonic frequency at $f=2n$ kHz (n: integer)) of (a) plasma current I_ϕ/V_ϕ, (b) soft X ray emissivity I_{sx}/V_ϕ measured from minor radius $r=-12$ to 12 cm and (c) CrI intensity near the wall I_{CrI}/V_ϕ for the same condition of Fig. 10. Here, normalization is done by V_ϕ and 0 dB is taken at 2 kHz for each signal.

The growth time of resistive tearing mode of a few hundreds of μsec is nearly the same with a typical relaxation time in ZT-40M RFP plasma. This time is shorter than one modulation period of 500 μsec and longer than the characteristic time of the higher harmonics. Note that the classical skin time and poloidal Alfven time are several tens of msec and several μsec, respectively.

For the anti-driven case, the same feature with the drive case is also found, but the increasing rate of the soft X ray emissivity with the frequency is somewhat larger.

When we increase the Θ value to more than 1.6 for the case of F-Θ pumping, giant sawteeth of soft X rays at 1 kHz appear, similar to those reported in ref. 17 without the modulation. At the same time, a harmonic component at 3 kHz is also found due to the coupling of the 1 kHz sawtooth mode and the 2 kHz F-Θ modulation. The relative amplitude of 1 kHz is larger than that of 2 kHz for the outer plasma region, and smaller near the plasma center. In accordance with this, the F-Θ trajectory is different from the case for low Θ operation ($\Theta < 1.6$). The excursion period is 1 kHz due to the giant sawteeth. Therefore, at the first single cycle of 2 kHz modulation, the trajectory is the same with that for the drive case (see Fig. 4(a)), though the total arc length is somewhat smaller. At the next cycle of 2 kHz modulation, the trace shows an ellipse with clockwise rotation.

Phases between various modulated plasma parameters are examined for the drive and anti-drive cases at the fundamental frequency of 2 kHz (see also the description of Fig. 9 near the end of §2). In both cases, Θ value, plasma current I_ϕ and soft X ray emissivity I_{sx} (the peak of the emission near the plasma center is a little earlier than that near the plasma boundary) are nearly in phase with each other. Parameters of a_{eff}, α and η_k are nearly in phase opposition to the above plasma parameters. The phase for the impurity intensity of CrI and $B_{\phi w}$ and also the phase for the Poynting vector P and V_ϕ are nearly the same. The toroidal flux is in phase opposition to the poloidal flux for the drive case (nearly linear polarization), but an elliptic polarization is found for the anti-drive case.

It is shown from Fig. 12 that the plasma wall interaction increases with the frequency, i.e., soft X ray intensity near the plasma boundary and CrI intensity near the wall increase, and the fast penetration of plasma parameters are observed even at the higher frequency of >10 kHz. Therefore, a reduction of the higher harmonic components seems to be desirable to decrease the radiated power loss and the offset of F-Θ pumping effects. However, the generation mechanism of the higher harmonics due to the nonlinear coupling must be investigated before trying to control the harmonic components.

§4. Conclusions

In the reversed field pinch device ZT-40M, preliminary experiments on F-Θ pumping have been performed, and a possibility of the steady-state current drive has been suggested, provided that the plasma resistance does not increase significantly during modulation. Experimental results of the current and anti-current drives are in good agreement with the simulation results.

Plasma parameters depend on the phase δ between the toroidal and poloidal loop voltages with modulation frequencies of 1.3 and 2 kHz. Slight changes of plasma parameters are found for the current drive direction in comparison to the case without the modulation. However, for the anti-drive phasing, the increases in total radiated power and impurity intensity are observed with decreases in the plasma current and soft X ray intensity. During the modulation, changes of the break point radius α and minor radius a_{eff} are $\sim \pm(12\text{–}18)\%$ and $\sim \pm(5\text{–}7)\%$, respectively, and both of them are in phase opposition to the plasma current. Internal plasma structures with the use of MBFM and phases between plasma parameters are also studied.

Frequency spectra which have up to the 10th harmonics of the driving frequency have been analyzed, and I_ϕ / V_ϕ does not change with the frequency. On the other hand, the impurity intensity and soft X ray emissivity increase especially near the outer plasma region with the increase in the frequency, which indicates enhanced (strong) interaction between the wall and plasma surface. The fast penetra-

tion (>10 kHz) of changes in plasma parameters to the central plasma region is found.

The next needed experiments in order to explore the physics and technology issues relevant to evaluating *F-Θ* pumping as a steady-state current drive are as follows; 1) optimization of operation parameters such as $B_{\phi w}$, f and δ with a reduction of the plasma-wall interaction, 2) increasing the applied toroidal loop voltage to obtain an increase in the plasma current, 3) to examine plasma behavior and scaling.

Acknowledgements

The authors wish to thank the ZT-40M physics and engineering staff for the experimental operation and measurements, and in particular, Dr. D. M. Weldon for operation and Dr. J. A. Phillips for useful discussion.

This work was supported by the U.S. Department of Energy and the Japanese Ministry of Education on the agreement on Fusion Cooperation Program.

References

1) T. Ohkawa: Nucl. Fusion **10** (1970) 135.
2) N. J. Fisch and A. H. Boozer: Phys. Rev. Lett. **45** (1980) 720.
3) J. G. Cordey: Plasma Phys. and Controlled Fusion **26** (1984) 123.
4) C. N. Lashmore-Davies: in *Proc. of 5th Int. Workshop on ECE & ECH* (San Diego, 1985), Report No. GA-A18294, p. 264.
5) T. Maekawa, S. Tanaka, K. Ogawa, H. Gesso, H. Kikuchi, K. Saito and S. Shiina: in *Proc. of Trilateral Workshop on RFP Research* (Padua, 1987) p. 53.
6) M. K. Bevir and J. W. Gray: in *Proc. of the Reversed Field Pinch Theory Workshop* (LANL, Los Alamos, 1981), Report No. LA-8944-C, p. 176.
7) K. F. Schoenberg, R. F. Gribble and D. A. Baker: J. Appl. Phys. **56** (1984) 2519.
8) T. H. Jensen and M. S. Chu: Phys. Fluids **27** (1984) 2881.
9) K. F. Schoenberg, C. J. Buchenauer, R. S. Massey, J. G. Melton, R. W. Moses, Jr., R. A. Nebel and J. A. Phillips: Phys. Fluids **27** (1984) 548.
10) K. F. Schoenberg, C. P. Munson, T. E. Cayton, J. N. Downing, P. G. Weber, G. A. Wurden, D. A. Baker, C. J. Buchenauer, L. C. Burkhardt, J. N. DiMarco, R. M. Erickson, P. R. Forman, A. Haberstich, R. B. Howell, J. C. Ingraham, R. S. Massey, G. Miller, R. W. Moses, R. A. Nebel, J. A. Phillips, M. M. Pickrell, A. E. Schofield, R. G. Watt and D. M. Weldon: in *Plasma Physics and Controlled Nuclear Fusion Research* 1986 (Proc. 11th Int. Conf. Kyoto, 1986), IAEA, Vienna (1987) Vol. 2, p. 423.
11) K. F. Schoenberg, J. C. Ingraham, C. P. Munson, P. G. Weber, D. A. Baker, R. F. Gribble, R. B. Howell, G. Miller, W. A. Reass, A. E. Schofield, S. Shinohara and G. A. Wurden: Phys. Fluids **31** (1988) 2285.
12) G. Miller, J. C. Ingraham and L. S. Schrank: Rev. Sci. Instrum. **53** (1982) 1410.
13) K. F. Schoenberg, R. W. Moses, Jr. and R. L. Hagenson: Phys. Fluids **27** (1984) 1671.
14) D. A. Baker, C. J. Buchenauer, L. C. Burkhardt, E. J. Caramana, J. N. DiMarco, J. N. Downing, R. M. Erickson, R. F. Gribble, A. Haberstich, R. B. Howell, J. C. Ingraham, A. R. Jacobson, K. A. Klare, E. M. Little, R. S. Massey, J. G. Melton, G. Miller, R. W. Moses, C. P. Munson, J. A. Phillips, M. M. Pickrell, R. A. Nebel, A. E. Schofield, K. F. Schoenberg, R. G. Watt, P. G. Weber, D. M. Weldon, K. A. Werley, R. W. Wilkins and G. A. Wurden: in *Plasma Physics and Controlled Nuclear Fusion Research* 1984 (Proc. 10th Int. Conf. London, 1984), IAEA, Vienna (1985) Vol. 2, p. 439.
15) G. A. Wurden: Phys. Fluids **27** (1984) 551.
16) K. F. Schoenberg, R. F. Gribble and J. A. Phillips: Nucl. Fusion **22** (1982) 1433.
17) R. G. Watt and E. M. Little: Phys. Fluids **27** (1984) 784.